Available online at www.sciencedirect.com
ScienceDirect
Journal of Power Sources 174 (2007) 592–597
JOURNAL OF POWER SOURCES
www.elsevier.com/locate/jpowsour

Short communication

A study on insertion/removal kinetics of lithium ion in $LiCr_xMn_{2-x}O_4$ by using powder microelectrode

R.H. Zeng, W.S. Li *, D.S. Lu, Q.M. Huang

Department of Chemistry, South China Normal University, Guangzhou 510631, China

Available online 27 June 2007

Abstract

The insertion/removal processes of lithium ion in chromium doped spinel lithium manganese oxide ($LiCr_xMn_{2-x}O_4$) were studied with electrochemical impedance spectroscopy (EIS) on a powder microelectrode, as well as X-ray diffraction (XRD) and cyclic voltammetry (CV), and was compared with those of pure spinel lithium manganese oxide ($LiMn_2O_4$). The insertion/removal process of lithium ion in the spinel oxides consists of three steps: charge transfer of lithium ion on the surface of the spinel oxides, diffusion and occupation of lithium ion in the lattice of the spinel oxide. The doping of chromium in spinel lithium manganese oxide results in the increase of the charge transfer resistance and the double layer capacitance for lithium insertion or removal and the decrease of the diffusion coefficient of lithium ion in the lattice of spinel oxide. However, the insertion capacitance, a parameter reflecting the occupation of lithium ion in the lattice of the spinel oxide, is hardly influenced by the doping of chromium. The influence of the doped chromium on the kinetic process of lithium insertion/removal in spinel lithium manganese oxide is related to the contraction of spinel lattice due to the doping.

Keywords: Insertion and removal kinetics; Spinel lithium manganese dioxide; Doping; Chromium

1. Introduction

Manganese oxides are useful cathode materials of primary and secondary materials, because they are less toxic and abundant in nature [1,2]. The most important manganese oxide is spinel lithium manganese oxide, $LiMn_2O_4$, used as the cathode materials for lithium ion battery, which is easy to prepare and has high capacity density [3–5]. However, its application is limited by its instability due to Jahn–Teller effect and dissolution of manganese into electrolyte during cycling of charging and discharge [6–8]. The problem can be solved to a great extent by substitution of other elements such as chromium, cobalt and nickel for a small fraction of manganese atoms in spinel lattice [9–15]. Much work has been done on preparation, structure and cyclic stability of doped spinel lithium manganese oxides, but less knowledge is available on the effect of doped elements on the kinetics of lithium insertion and removal in the spinel oxide, which is essential for the understanding of stability improvement and for the better application of doped lithium manganese oxide.

In this work, spinel lithium manganese oxides with and without the doping of chromium are synthesized by sol–gel method, then their crystal structure and cyclic stability are characterized with X-ray diffraction (XRD) and cyclic voltammetry (CV), at last the kinetic process of lithium ion in the prepared samples are studied on a powder microelectrode with electrochemical impedance spectroscopy.

2. Experimental

Three samples, $LiMn_2O_4$, $LiCr_{0.16}Mn_{1.84}O_4$ and $LiCr_{0.25}Mn_{1.75}O_4$, were synthesized by sol–gel method with $CH_3COOLi{\cdot}2H_2O$, $Mn(CH_3COO)_2$, $Cr(NO_3)_3{\cdot}9H_2O$, and $(C_6H_8O_7{\cdot}7H_2O)$ in the ratios of 1:2:0:3, 1:1.84:0.16:3 and 1:1.75:0.25:3, respectively. Aqueous solution with $CH_3COOLi{\cdot}2H_2O$ and $Cr(NO_3)_3{\cdot}9H_2O$ was added into $Mn(CH_3COO)_2$ saturated solution under stirring. Then $(C_6H_8O_7{\cdot}7H_2O)$ solution was added to obtain a mixture solution with lithium, manganese and chromium. The mixture solution was mediated with aqueous concentrated NH_3 solution to pH 6.3 and kept at 80 °C under stirring till a dry precursor was obtained. The precursor was heated to 500 °C with 1 °C min^{-1} and kept at 500 °C for 12 h to remove organic compounds and then heated to 750 °C with

* Corresponding author. Tel.: +86 20 39310256; fax: +86 20 39310256.
E-mail address: liwsh@scnu.edu.cn (W.S. Li).

0378-7753/$ – see front matter © 2007 Elsevier B.V. All rights reserved.
doi:10.1016/j.jpowsour.2007.06.120

1 °C min^{-1} and kept at 750 °C for 72 h to obtain the samples. All the chemicals were analytic grade.

XRD was conducted on a D/MAX-3A/Rigaku diffractor with Cu Kα radiation of 30 kV, 30 mA at 12° min^{-1}. The cell constant a of the spinel oxide was obtained with

$$a = \frac{d}{(h^2 + k^2 + l^2)^{-0.5}} \quad (1)$$

where h, k and l are the indexes of crystal place and d the distance between crystal planes. The volume of the spinel cell V was obtained with

$$V = a^3 \quad (2)$$

The length R (Å) of Mn–O and Mn–Mn was obtained with

$$R_{\text{Mn–Mn}} = \frac{2^{0.5}a}{4} \quad (3)$$

$$R_{\text{Mn–O}} = a(3u^2 - 2u + 0.375)^{0.5} \quad (4)$$

where u is the position constant of oxygen in the spinel lattice and equal to 0.265.

Electrochemical experiments were performed with PGSTAT-30 (Autolab) in a two-electrode cell with powder microelectrode as the working electrode and metal lithium as the counter electrode and the reference electrode. The electrolyte was 1 M $LiPF_6$-EC + EMC + DMC (m_{EC}:m_{EMC}:m_{DMC} = 1:1:1, Merck). The electrolyte cell was set up in a glove box under argon atmosphere. The powder microelectrode was prepared as follows [16,17]. A platinum (99.995% Pt) wire with a diameter of 100 μm was sealed in a glass tube to obtain a platinum microdisk electrode. The microdisk electrode was etched in a mixed concentrated acid solution for 30 min to obtain a microcavity electrode. The cavity electrode was ground on a glass plate with the mixture powder of sample and graphite (1:1 in wt.) to obtain the powder microelectrode.

3. Results and discussion

Fig. 1 shows the XRD pattern of three samples. It can be found that the diffractions of three samples are characteristic of spinel crystal structure, in which lithium ions occupy the 16a positions of tetrahedra, manganese ions (Mn^{3+} and Mn^{4+}) occupy the 16d positions of octahedra and oxygen ions occupy the 32e positions, the vertices of tetrahedral and octahedra. The same diffractions of spinel structure for the samples with and without doping indicate that the doped chromium has entered the lattice of 16d positions to replace manganese.

The cell parameters calculated with Eqs. (1)–(4) based on the diffraction peak of Fig. 1 are listed in Table 1. It can be seen from Table 1 that the cell constant, the volume and the bond length of spinel lithium manganese oxide become small due to the doping of chromium and become smaller as the chromium contents increase, indicating that spinel cell of lithium manganese oxide was contracted due to the doping of chromium. This effect can be ascribed to the bond of Cr–O is stronger than that of Mn–O.

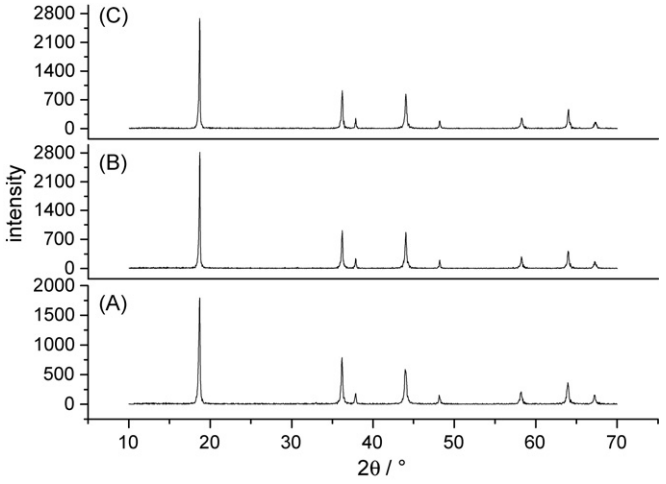

Fig. 1. XRD pattern of samples: (A) $LiMn_2O_4$, (B) $LiCr_{0.16}Mn_{1.84}O_4$, and (C) $LiCr_{0.25}Mn_{1.75}O_4$.

Fig. 2 shows the voltammograms of three samples obtained with slow potential sweep during the first cycle. It can be seen that two steps for lithium insertion and removal in the spinel oxide can be separated significantly for the sample with and without the doping of chromium. However, There are differences in the voltammograms between the samples with and without the doping of chromium.

First, the charging and discharge efficiency is different. Charging and discharge efficiency, the ratio of electric quantity of charging and discharge obtained by integrating forward or backward scan voltammogram, is 95%, 98% and 100% for the samples $LiMn_2O_4$, $LiCr_{0.16}Mn_{1.84}O_4$ and $LiCr_{0.25}Mn_{1.75}O_4$, respectively. The charging and discharge efficiency increases with increasing chromium content in the spinel oxide, indicating that irreversible capacity loss of spinel lithium manganese oxide is reduced by the doping of chromium.

Secondly, the amount of lithium insertion and removal for each of two steps, which can be obtained from the integration of the oxidation or reduction peak, is different. As shown in Fig. 2A, the amount of lithium insertion and removal at low potential is almost equal to that at high potential. However, the amount of lithium insertion and removal increases at low potential and decreases at high potential due to the doping of chromium, as shown in Fig. 2B and C. This suggests that the doping of chromium in the spinel lithium manganese oxide changes the amount of lithium insertion and removal for each of two steps.

To understand the cyclic stability of the doped lithium manganese oxide, cyclic voltammograms of three samples were

Table 1
Cell parameters of spinel samples with and without doping

Samples	a (Å)	V (Å^3)	$R_{\text{Mn–Mn}}$ (Å)	$R_{\text{Mn–O}}$ (Å)
$LiMn_2O_4$	8.2275	556.93	2.9089	1.9413
$LiCr_{0.16}Mn_{1.84}O_4$	8.2261	556.65	2.9084	1.9410
$LiCr_{0.25}Mn_{1.75}O_4$	8.2243	556.28	2.9077	1.9406

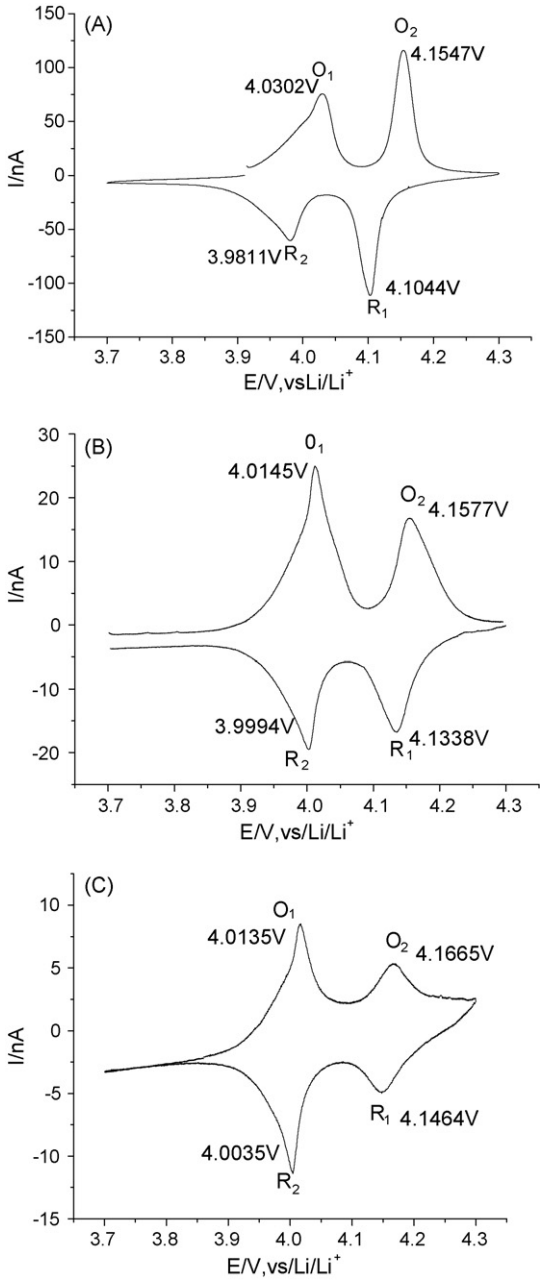

Fig. 2. Cyclic voltammograms of samples on powder microelectrode: (A) $LiMn_2O_4$, (B) $LiCr_{0.16}Mn_{1.84}O_4$, and (C) $LiCr_{0.25}Mn_{1.75}O_4$; scan rate: $80\,\mu V\,s^{-1}$.

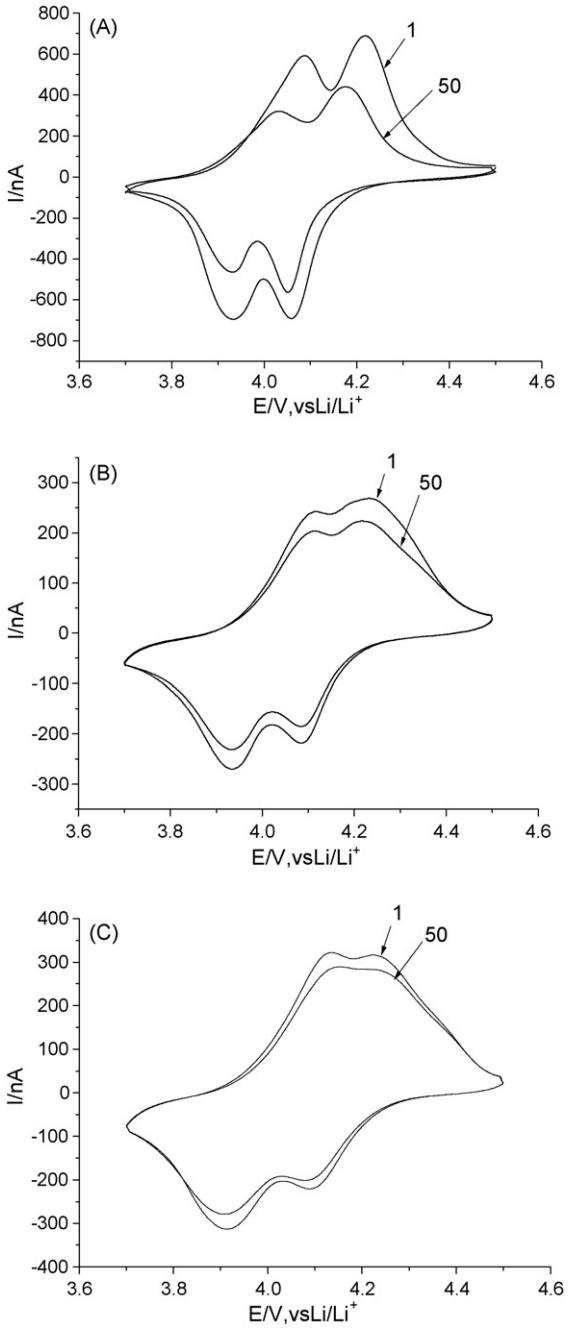

Fig. 3. Cyclic voltammograms of samples on powder microelectrode: (A) $LiMn_2O_4$, (B) $LiCr_{0.16}Mn_{1.84}O_4$, and (C) $LiCr_{0.25}Mn_{1.75}O_4$; scan rate: $2\,mV\,s^{-1}$.

measured on powder microelectrodes with a faster scan rate. The voltammograms of the first and the 50th cycles are shown in Fig. 3. It can be found from Fig. 3 that the peak currents of the spinel oxide without doping decrease more quickly than those of the spinel oxides with doping. After 50 cycles, the discharge capacity, obtained by integrating the backward scanning voltammogram, becomes 30.7%, 19.3% and 11.7% of that at the first cycle for the samples $LiMn_2O_4$, $LiCr_{0.16}Mn_{1.84}O_4$ and $LiCr_{0.25}Mn_{1.75}O_4$, respectively. It is apparent that the cyclic stability of spinel lithium manganese oxide can be improved by the doping of chromium. Similar results have been obtained for the doping of elements other than chromium and this effect can be ascribed to the stability improvement of the spinel oxide by the doping of elements [18,19].

Electrochemical impedance spectroscopy was used to understand the kinetic process of lithium ion in samples. Before the EIS measurement, the powder microelectrode was charged with a constant current of 15 nA to 4.3 V and kept at 4.3 V till the current was lower than 10 pA. The measurement begun after potentiostat at each measured potential for 30 min. The frequency range used was from 100 KHz to 5 mHz and with an amplitude of 5 mV.

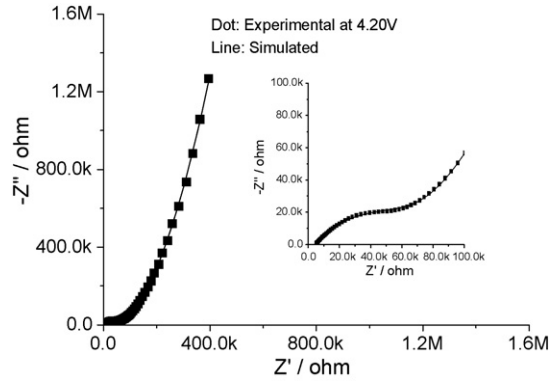

Fig. 4. Nyquist plot of sample $LiMn_2O_4$ on powder microelectrode.

Fig. 4 shows the Nyquist plot of the sample without the doping of chromium. It can be found that the Nyquist plot is composed of three part: semicircle at high frequency, straight line with a smaller slope at middle frequency and straight line with a bigger slope at low frequency. The semicircle at high frequency is corresponding to a charge transfer step, which should be ascribed to the charge transfer of lithium ion on the surface of spinel oxide because there are no other electrode reactions taking place during lithium insertion and removal in the spinel oxide. The straight line at middle frequency is corresponding to a diffusion step, which can be ascribed to the diffusion of lithium in the lattice of the spinel oxide because the diffusion of lithium ion in electrolyte is fast and can be neglected in EIS compared to the diffusion of lithium in the lattice of the spinel. The straight line with high slope at low frequency belongs to a capacitance behavior and it should be ascribed to the insertion/removal capacitance of lithium in the lattice of the spinel oxide. Based on these considerations, the equivalent circuit of Fig. 5 can be used to describe the kinetic process of lithium in the spinel oxide.

In Fig. 5, R_s represents the solution resistance, C_{dl} the double layer capacitance, R_{ct} the resistance of charge transfer, Z_w Warburg impedance reflecting the diffusion process of lithium in the lattice of the spinel oxide and C_{int} insertion or removal capacitance reflecting the occupation process of lithium in lattice of the spinel oxide. The solid line in Fig. 4 is the result obtained by simulating the experimental result with the equivalent circuit of Fig. 5. It can be found that the experimental result can be well fitted and thus the kinetic parameters can be easily obtained by simulating.

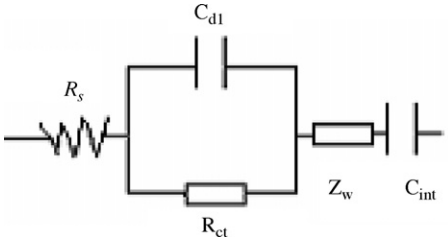

Fig. 5. Equivalent circuit describing the kinetic process of lithium in spinel lithium manganese oxide on powder microelectrode.

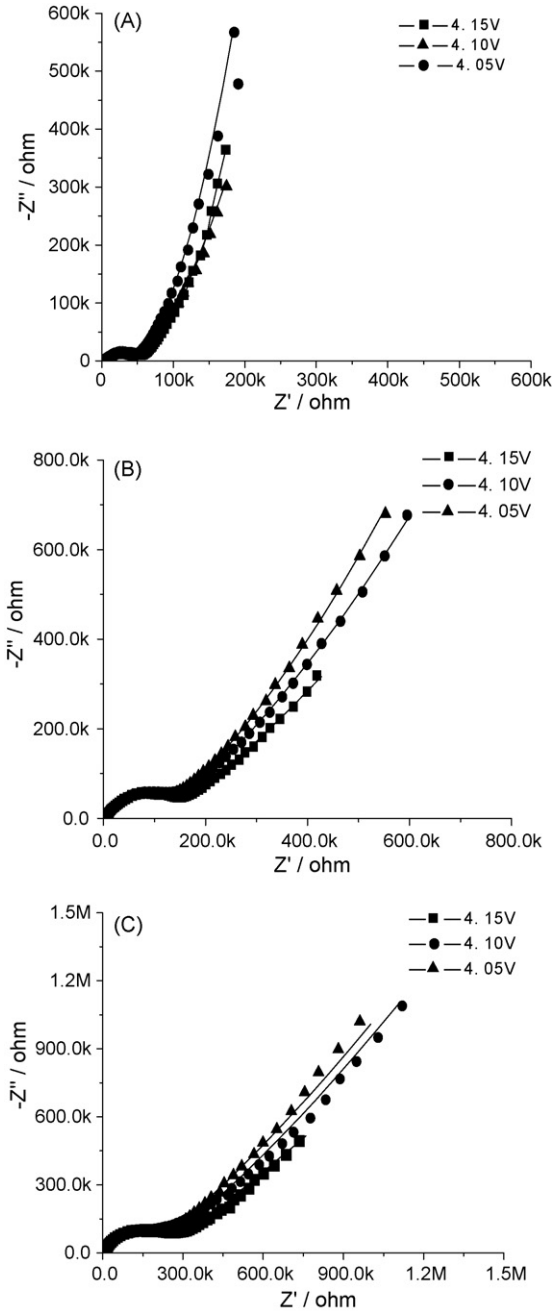

Fig. 6. Nyquist plots of samples on powder microelectrode at some potential: (A) $LiMn_2O_4$, (B) $LiCr_{0.16}Mn_{1.84}O_4$, and (C) $LiCr_{0.25}Mn_{1.75}O_4$; (▲, ■, ●) experimental, (—) simulated.

The electrochemical impedance of the samples with and without the doping of chromium was measured under the potentials every 50 mV from 4.2 to 3.85 V. Fig. 6 shows the results of three samples under 4.15, 4.10 and 4.05 V. As shown in the Fig. 4, the dots and the lines in Fig. 6 represent the experimental and simulated results, respectively. It can be found that the Nyquist plots are similar for the samples with and without the doping of chromium and can be well fitted by the equivalent circuit of Fig. 5. The parameters of three samples under different potentials, R_s, C_{dl}, R_{ct}, Z_w, and C_{int} can be obtained by simulating the measured electrochemical impedance with the equivalent circuit of Fig. 5.

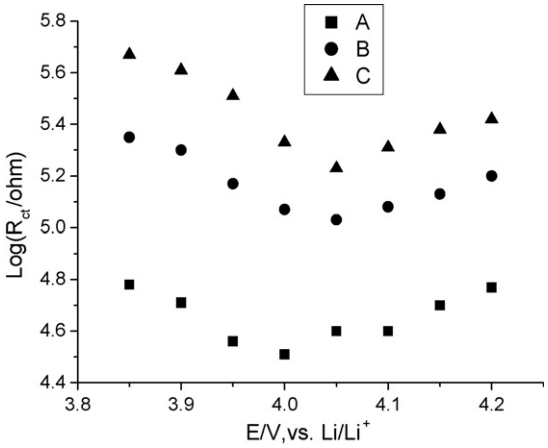

Fig. 7. The dependence of charge transfer resistance with potential for lithium insertion and removal in samples: (A) $LiMn_2O_4$, (B) $LiCr_{0.16}Mn_{1.84}O_4$, and (C) $LiCr_{0.25}Mn_{1.75}O_4$.

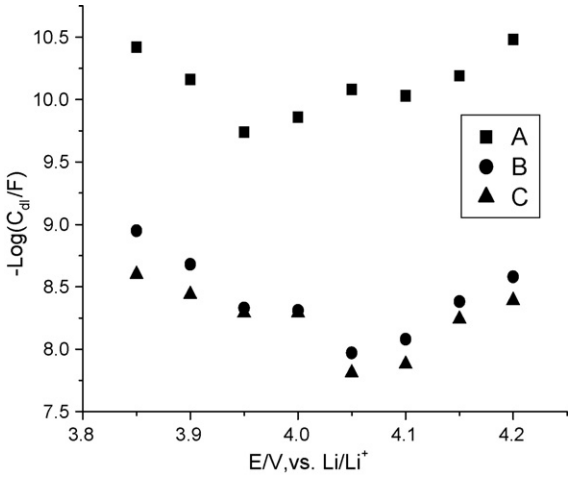

Fig. 8. The dependence of double layer capacitance with potential for lithium insertion and removal in samples: (A) $LiMn_2O_4$, (B) $LiCr_{0.16}Mn_{1.84}O_4$, and (C) $LiCr_{0.25}Mn_{1.75}O_4$.

Fig. 7 shows the dependence of charge transfer resistance R_{ct} with the potential. It can be found that the charge transfer resistance for lithium insertion and removal in the samples with and without doping of chromium is influenced by the potential and its dependence on potential is the same for the samples with and without the doping of chromium. There is a minimum charge transfer resistance for all the samples, which is at the potential in between the two peak potentials for two steps of lithium insertion and removal, about 4.0 V for the sample without the doping of chromium and 4.05 V for the samples with the doping of chromium, as shown in Fig. 2. The charge transfer resistance increases for all samples as the potential increases or decreases from the potential where the charge transfer resistance is in its minimum value. Comparing the samples with and without doping of chromium, it can be seen that the charge transfer resistance increases from the sample without doping to the sample with doping. There is about a decade of increase in charge transfer resistance due to the doping of chromium and as the content of doped chromium in spinel oxide increases the charge transfer resistance increases.

Fig. 8 shows the dependence of double layer capacitance with the potential. It can be found that the double layer capacitance for lithium insertion and removal in the samples with and without the doping of chromium is also influenced by the potential and its dependence on potential is also the same for the samples with and without the doping of chromium. Similar to the change of charge transfer resistance that has a minimum, there is a maximum double layer capacitance for all the samples, which is also at the potential in between the two peak potentials for two steps of lithium insertion and removal, about 4.0 V for the sample without the doping of chromium and 4.05 V for the samples with the doping of chromium. The double layer capacitance decreases for all samples as the potential increases or decreases from the potential where the double layer capacitance is in its maximum value. Comparing the samples with and without the doping of chromium, it can be seen that the double layer capacitance also increases from the sample without doping to the sample with doping. There also is about a decade of increase in double layer capacitance due to the doping of chromium. Different from the effect of chromium on the charge transfer resistance, however, the double layer capacitance of doped spinel oxide is almost independent of the content of doped chromium.

To obtain the diffusion parameter of lithium in the lattice of the samples, a simplified treatment is made. The diffusion coefficient D_{Li} of lithium in the lattice of spinel lattice can be expressed as [3]

$$D_{Li} = \frac{1}{\sigma^4}\frac{R^4T^4}{4A^4n^8F^8c^2} = \kappa\frac{1}{\sigma^4} \quad (5)$$

where σ is obtained by simulating experimental electrochemical impedance with the equivalent circuit of Fig. 5, A the surface area of the samples, n the electron number in the charge transfer step, T the temperature, R the gas constant and F is the Faradaic constant. Under the same temperature, A, n, T, R and F are considered to be constants and the same for all samples, thus they can be put together to be a constant k.

The dependence of diffusion coefficients of lithium in lattice of three samples obtained from Eq. (5) is shown in Fig. 9. It can be found that the diffusion coefficients of lithium in lattice of the samples with and without the doping of chromium increases with potential when potential is lower than 4.0 V but is less dependent on the potential when potential is higher than 4.0 V. Comparing the samples with and without the doping of chromium, it can be seen that the diffusion coefficient of spinel lithium manganese oxide becomes smaller due to the doping of chromium.

Fig. 10 shows the dependence of insertion capacitance with the potential. It can be found that the insertion capacitance for the occupation of lithium in the lattice of samples with and without the doping of chromium is hardly influenced by potential except for the potentials near the potential in between the two peak potentials for two steps of lithium insertion and removal, where the insertion capacitance reaches a higher value. Different from the behaviors of double layer capacitance behavior, the insertion capacitance is hardly influenced by the doping of chromium.

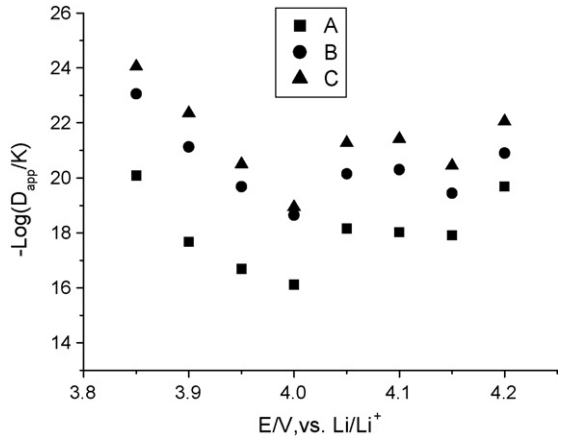

Fig. 9. The dependence of diffusion coefficient with potential for lithium insertion and removal in samples: (A) $LiMn_2O_4$, (B) $LiCr_{0.16}Mn_{1.84}O_4$, and (C) $LiCr_{0.25}Mn_{1.75}O_4$.

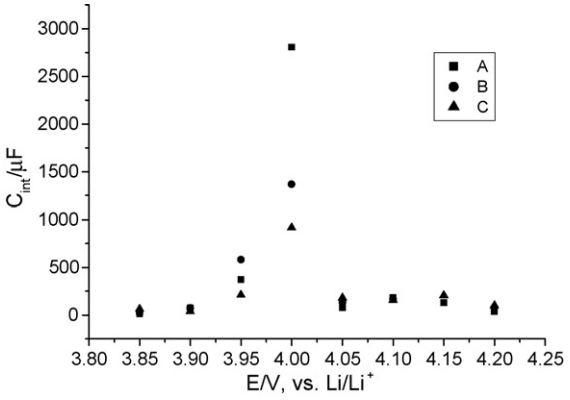

Fig. 10. The dependence of insertion capacitance with potential for lithium insertion and removal in samples: (A) $LiMn_2O_4$, (B) $LiCr_{0.16}Mn_{1.84}O_4$, and (C) $LiCr_{0.25}Mn_{1.75}O_4$.

The effect of doped chromium on the charge transfer resistance, the double layer capacitance and the diffusion coefficient must be related to the lattice contraction of spinel lithium manganese oxide due to the doping. However, the lattice contraction of spinel lithium manganese oxide does not affect the occupation of lithium in the spinel lattice.

4. Conclusion

Chromium can enter the lattice of spinel lithium manganese oxdie forming chromium doped spinel oxide $LiCr_xMn_{2-x}O_4$, resulting in the change of kinetic parameters. Due to the doping of chromium in the spinel oxide, the volume of spinel oxide is contracted, the charge transfer resistance and the double layer capacitance for lithium insertion or removal increase, and the diffusion coefficient of lithium in the lattice of spinel oxide decreases. However, the insertion capacitance of lithium in the spinel lattice is hardly influenced by the doping of chromium.

Acknowledgements

This work was financially supported by NSFC (20373016), EYTP of MOE, Key project of Guangdong Province (2004A11001001) and Guangzhou City (2004Z3-D0091).

References

[1] W.S. Li, L.C. Jiang, G.Y. Xie, et al., J. Power Sources 58 (1996) 235.
[2] W.S. Li, L.C. Jiang, Z.T. Huang, J. Power Sources 69 (1997) 81.
[3] C.J. Curtis, J.X. Wang, D.L. Schulz, J. Electrochem. Soc. 151 (2004) A590.
[4] J.M. Tarascon, M. Armand, Nature 414 (2001) 359.
[5] S. Bach, J. Farcy, J.P. Pereira-Ramos, Solid State Ionics 110 (1998) 193.
[6] D. Aurbach, M.D. Levi, E. Levi, et al., J. Electrochem. Soc. 145 (1998) 3024.
[7] M.D. Levi, K. Gamulski, D. Aurbach, et al., J. Electrochem. Soc. 147 (2000) 25.
[8] D. Aurbach, M.D. Levi, K. Gamulski, J Power Sources 81–82 (1999) 472.
[9] I.S. Jeng, J.U. Kim, H.B. Gu, J. Power Sources 102 (2001) 55.
[10] M. Mohamedi, K. Makino, K. Dokko, et al., Electrochim. Acta 48 (2002) 79.
[11] G.T.K. Fey, C.Z. Lu, T.P. Kumar, J. Power Sources 115 (2003) 332.
[12] H.J. Bang, V.S. Donepudi, J. Prakash, Electrochim. Acta 48 (2002) 443.
[13] A.D. Robertson, S.H. Lu, W.F. Howard, J. Electrochem. Soc. 144 (1997) 3505.
[14] C. Sigala, A.L.G.L. Salle, Y. Piffard, J. Electrochem. Soc. 144 (2003) A812.
[15] J.R. Dahn, T. Zheng, C.L. Thomas, J. Electrochem. Soc. 145 (1998) 851.
[16] D.S. Lu, W.S. Li, Acta Chim. Sin. 61 (2003) 225.
[17] D.S. Lu, W.S. Li, Chin. J. Inorg. Mater. 19 (2004) 801.
[18] P. Arora, B.N. Popov, R.E. White, J. Electrochem. Soc. 145 (1998) 807.
[19] G.H. Li, H. Ikuta, T. Uchida, et al., J. Electrochem. Soc. 143 (1996) 178.